Proceedings of the 21st ICSMGE, Vienna, Austria, 14 – 19 June 2026. Pistrol, Adam & Schweiger (eds.)
Published by: ÖGG, Austrian Society for Geomechanics, Salzburg, Austria, ISBN 978-3-9503898-4-5
https://doi.org/10.53243/ICSMGE2026-271

A 3D finite element model of rockfill saturation collapse in tailings dams

Nicolas A. Labanda
Principal Tailings Engineer, Mine Waste, WSP, Australia, nicolas.labanda@wsp.com

Roberto J. Cier
Senior Associate Engineer, ATC Williams, Australia, robertoc@atcwilliams.com

Felipe L. Rivarola
Senior Tailings Engineer, Mine Waste, WSP, Argentina, felipe.lopez1@wsp.com

ABSTRACT: Mining companies have been working to understand different phenomena related to tailings facilities and their performance, mainly motivated by the latest advancements in their regulations and standards due to recent failures of these structures around the world. This interest, along with the increasing access to more powerful computational resources, has driven the development of more complex numerical assessments to support forensic studies that allow estimating and predicting historical and future behavior under different scenarios. This study presents a three-dimensional numerical model developed for a downstream tailings storage facility (TSF) which has been undergoing historical cracking episodes due to volumetric collapse of a portion of the rockfill comprising its embankment. The authors conducted this numerical analysis to simulate a series of localized deformation features appearing at various locations in the TSF. A hydromechanical finite element model was developed along with an in-house constitutive model that accounts for the volumetric contraction caused by increased saturation, typically presented in loose coarse-graded materials.

KEYWORDS: tailings storage facilities, volumetric contraction, collapse, rockfill, finite elements.

1 INTRODUCTION

Dumped rockfill, typically derived from mine waste rock or borrow areas near the mine site, is one of the primary construction materials selected in the design of TSF embankments. It optimizes material handling quantities and costs, and allows recycling onsite waste streams, minimizing the environmental impact of mining operations. Despite these benefits, dumped rockfill also causes significant engineering issues. This type of material presents potential for internal instability, particle migration and suffusion, whereas its saturation may generate high settlements and movements. This is because dumped rockfill, when loosely placed, is found to develop particles rearrangements under hydromechanical effects, which are time-dependent when the rockfill is loaded or wet. Rockfill materials can accumulate deformation over decades and experience volumetric collapse when partially saturated, submerged, or subjected to sudden water content changes, such as in rainfall events. The collapse is mainly due to particle cracking, which is initiated from stress concentrations at interparticle contacts under loading and/or water ingress. These mechanisms have been widely studied in the literature (Sowers et al., 1965; Marsal, 1973; Oldecop & Alonso, 2001; Oldecop & Alonso, 2004).

This study presents a three-dimensional deformation model of a downstream-raised tailings storage facility (TSF) constructed using dumped rockfill. A user-defined constitutive model was developed and implemented in PLAXIS to simulate the volumetric collapse of the rockfill upon wetting. The model was calibrated against laboratory test data to validate its predictive capability. The geometry, construction sequence, and hydraulic conditions of the TSF were modeled using site-specific information derived from aerial imagery, topographic surveys, as well as historical design and construction records. This comprehensive dataset enabled the model to realistically reproduce TSF's chronological deformation behavior and to provide insights into its potential future performance under evolving loading and environmental conditions. Simulation results included predictions of cracking and deformation patterns. Key findings are discussed, along with their implications for future design, assessment, and monitoring of TSFs.

2 MODELLING OVERVIEW

A 3D model was constructed using the finite element package PLAXIS 3D v22. Figure 1 summarizes the staged construction, including the geotechnical units used for the raising simulation of the TSF. The simplified construction sequence was simulated as follows:

1. Initial topography using the pre-mining ground survey.
2. Starter embankment construction using 2m thick layers from ground level to reference level (RL) 573 m, including compaction stage.
3. Loosely placed rockfill disposal using 5 to 10m thick layers to RL 573 m.
4. Haul road construction using 5 m thick layers.
5. Tailings deposition to RL 562 m using 2 m thick layers.
6. First raise embankment construction using 2 m thick layers to RL 588 m, including compaction stage.
7. Tailings deposition using 2 m thick layers to RL 582 m.
8. Second raise embankment using 2 m thick layers to RL 605 m, including compaction.
9. Tailings deposition using 2 m thick layers to RL 602 m.

3 CONSTITUTIVE MODEL FOR ROCKFILL COLLAPSE

3.1 *Rockfill constitutive model*

A constitutive model was developed based on a family of constitutive models implemented in PLAXIS (Sottile et al., 2019) and expanded to consider saturation collapse in 3D. Table 1 summarizes the constitutive model inputs and the calculation workflow:

- Line 1 includes all input parameters including current saturation (S_i), start and end saturation (S_{start} and S_{end} respectively) where the volumetric collapse starts and finishes, and the maximum volumetric deformation that the material can develop ($\varepsilon_{v,max}$). The remaining parameters define the strength and stiffness of the

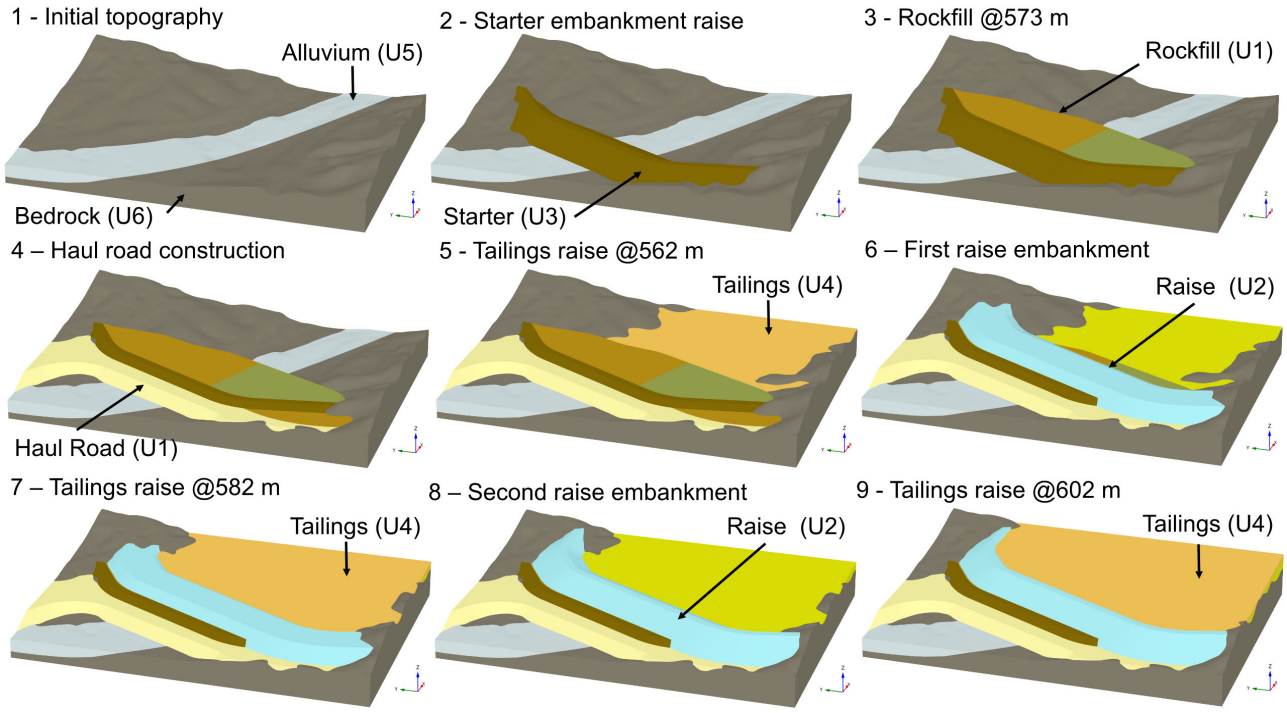

Figure 1. TSF staged construction.

material: ϕ and ψ are the friction angle and the dilatancy angle, respectively, whereas G_{ref}, ν and m are the shear stiffness modulus at a reference pressure, Poisson modulus and stiffness exponent (or Janbu's coefficient), respectively.

- Lines 2 to 11 update the volumetric deformation as a function of saturation, followed by Line 14 which updates the stiffness and strength parameters.

Lines 15 to 21 updates the stresses following an explicit algorithm as discussed in the literature (de Souza Neto et al., 2008; Sottile et al., 2019).

Table 1. Stress update algorithm including volumetric collapse.

Line	Description
1:	**Input:** $\boldsymbol{\sigma}_{n+1}^{(0)}, S_i, S_{start}, S_{end}, \varepsilon_{v,max}, \phi, \psi, G_{ref}, \nu, m$
2:	**if** $S_i \geq \max(S)$ **then**
3:	**if** $S_i < S_{start}$ **then**
4:	$\varepsilon_{v,col,i} \leftarrow 0\%$
5:	**else if** $S_i < S_{end}$ **then**
6:	$\varepsilon_{v,col,i} \leftarrow (S_{start} - S_i) \cdot \left(\frac{\varepsilon_{v,max}}{S_{end} - S_{start}}\right)$
7:	**else**
8:	$\varepsilon_{v,col,i} \leftarrow -\varepsilon_{v,max}$
9:	**end if**
10:	$\Delta\varepsilon_{v,col} \leftarrow \varepsilon_{v,col,i} - \varepsilon_{v,col,i-1}$
11:	**else**
12:	$\Delta\varepsilon_{v,col} \leftarrow 0\%$
13:	**end if**
14:	Update $G^{(i)}, \phi^{(i)}, \psi^{(i)}$
15:	Compute eigensystem of $\boldsymbol{\sigma}_{n+1}^{(i)}$
16:	**if** $f\left[\boldsymbol{\sigma}_{n+1}^{(i)}\right] \leq 0$ **then**
17:	**return**
18:	**else**
19:	Update $\boldsymbol{\sigma}_{n+1}^{(i)}$ using explicit Mohr-Coulomb stress update
20:	Set $i = i + 1$ and continue with the next (pseudo) timestep
21:	**end if**

3.2 *Rockfill laboratory testing outcomes*

A comprehensive laboratory testing campaign was conducted to study the behavior of the mine waste fill bulk samples under oedometric compression and shear stress paths. Three samples with different initial densities were analyzed. The first two of them entailed four vertical loading steps under air-dried condition; samples were then saturated and the wetting collapse under constant stress was recorded; finally, the samples were sheared to failure. For the third test, the sample was saturated after the second loading step, then two more loading steps were carried out at a saturated state and finally the sample was sheared. The sample achieved friction angles ϕ from 37 to 41 degrees. The lower value corresponds to large strains and represents the steady state, whereas the higher value corresponds to peak strength achieved at test 2 where some dilation ψ was achieved due to high pre-shearing densities and lower confining stresses. The wetting collapse occurs almost instantly after saturation. Minimum dry densities varied between 15.9 and 20.5 kN/m^3 whereas maximum dry densities varied between 21.0 and 27.6 kN/m^3.

For the sake of conciseness, lab testing results are not displayed in this paper and key results are summarized in Table 2, where σ_v' is the vertical effective stress at flooding, D_r is the relative density before flooding, $\varepsilon_{v,col}$ is the volumetric collapse after flooding, and ϕ is the peak friction angle.

Table 2. Summary of test conditions and key parameters.

Test	σ_v' [kPa]	D_r [%]	$\varepsilon_{v,col}$ [%]	ϕ [°]
1	1200	47.8	4.2	38
2	1000	84.8	1.6	41
3	600	51.0	3.2	37

3.3 *Rockfill calibration*

The stiffness parameter at the reference pressure G_{ref}, the Janbu's coefficient m, and the collapsibility potential were calibrated from the results of the laboratory tests described in Section 3.2. The calibration is shown in Figure 2, where the case of loose material was chosen as the most representative of the rockfill used on site. Additionally, Figure 3 shows the deviatoric stress versus strain curves, whereas Figure 4 displays the volume change versus axial strain curves for the user-defined material (USDM) and laboratory tests.

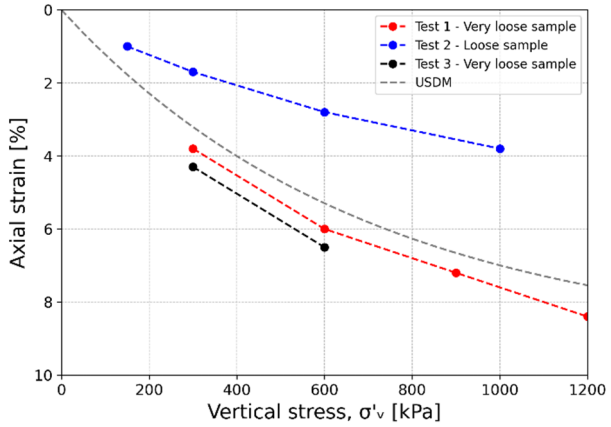

Figure 2. USDM stiffness calibration against lab testing results.

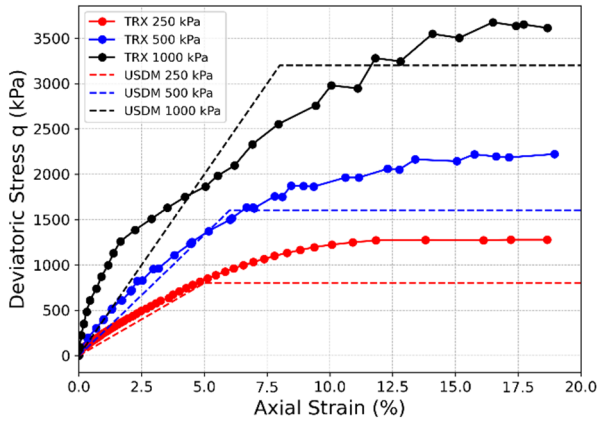

Figure 3. USDM strength calibration: Deviatoric stress vs axial strain.

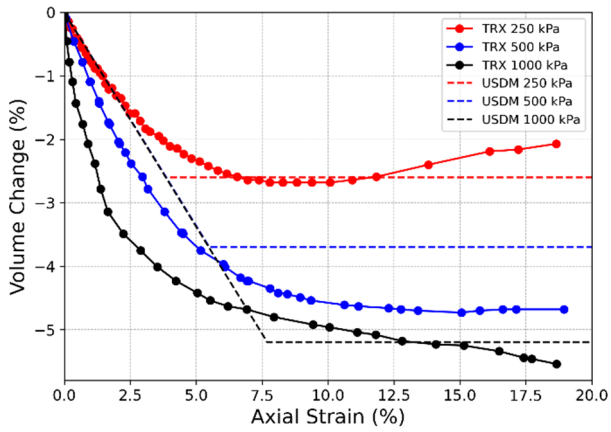

Figure 4. USDM strength calibration: volume change vs axial strain.

4 TSF MODEL CONSTRUCTION

The TSF construction was modelled using the sequence detailed in Section 2. Coupled groundwater flow and deformation analysis techniques were used. After the full rise of the dam, a long-term drying stage—including full drainage of the facility—was carried out to study how the reduction in pore water and the transition from submerged to dry density would promote further cracking propagation.

4.1 *Constitutive models and parameters*

The full list of geotechnical units presented in the model and selected constitutive models are detailed below:

- Unit 1 (U1): Rockfill (User-defined Material)
- Unit 2 (U2): Embankment Raises (Hardening Soil Small)
- Unit 3 (U3): Starter Embankment (Hardening Soil Small)
- Unit 4 (U4): Tailings (Linear Elastic)
- Unit 5 (U5): Alluvium/Colluvium (Hardening Soil Small)
- Unit 6 (U6): Bedrock (Linear Elastic)

Parameters are showed in Table 3. Given tailings strength is not contributing resistance on the overall stability, a simplistic linear elastic material was used to reduce computation time. Moreover, the calibration for the rest of the units was undertaken using site and laboratory testing. Details are intentionally omitted in this paper and uniquely key parameters are summarized.

Evidence and survey data indicated that, during the rockfill placement, a specific area was neither compacted nor subjected to vehicle traffic. As a result, this zone contains less competent material. The rockfill body was therefore divided into two distinct zones, each assigned a different maximum volumetric deformation to reflect its mechanical behavior. This differentiation plays a crucial role in the TSF's response throughout its construction. Figure 5 shows a detailed view of the rockfill body and its zoning.

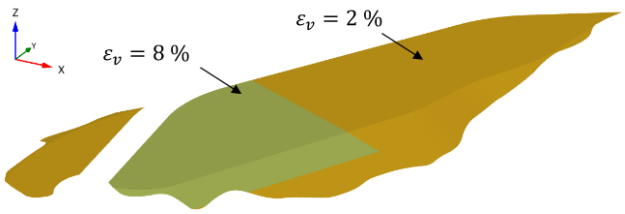

Figure 5. Rockfill body detail and zoning.

4.2 *Mesh and boundary conditions*

Figure 6 shows the full model at its final stage. The mesh comprised of 1,250,905 6-nodes tetrahedral elements with an average, maximum and minimum element size of 7.2 m, 46.9 m, and 0.1 m respectively.

Mechanical boundary conditions fixed the normal displacement on the four lateral boundaries of the model, whereas the bottom boundary of the model was modeled fully fixed.

Groundwater flow boundary conditions considered the downstream lateral boundaries of the model (at x_{min} and y_{max}) and the top boundary (surface) to be open, whereas the upstream lateral boundaries (at x_{max} and y_{min}) and the bottom boundary of the model were modeled closed.

Water table variation was simulated by imposing an influx on the tailings discharge line, as displayed in Figure 7. There, the black-shaded surface is the only zone where water was input into the system.

Table 3. Soil parameters across units.

Parameter	Symbol	Unit	U1	U2	U3	U4	U5	U6
Constitutive model	–	-	USDM	HSS	HSS	LE	HSS	LE
Unit weight	γ	kN/m^3	25	25	25	25	23	24
Effective cohesion	c'	kPa	1	0.5	-	-	-	-
Effective friction angle	ϕ'	°	37	32	37	-	-	-
Dilatancy angle	ψ	°	-	2	7	-	-	-
Reference pressure	p_{ref}	kPa	250	100	100	100	100	-
Reference shear modulus	G_{ref}	MPa	21	-	-	8.33	-	125
Reference small strain shear modulus	G_0^{ref}	MPa	-	115	115	-	180	-
Threshold shear strain	$\gamma_{0.7}$	-	-	3E-04	3E-04	-	1E-04	-
Unloading-reloading reference stiffness	E_{ur}^{ref}	MPa	-	90	90	-	150	-
Secant reference stiffness	E_{50}^{ref}	MPa	-	30	30	-	50	-
Oedometric reference stiffness	E_{oed}^{ref}	MPa	-	30	30	-	50	-
Stress-stiffness exponent	m	-	0.5	0.5	0.55	-	0.5	-
Unloading-reloading Poisson's ratio	ν_{ur}	-	0.2	0.2	0.2	-	0.2	0.2
Permeability	$k_h \vert k_v$	m/s	7.5E-04	1E-05	2.6E-05	5E-07	1E-04 | 1E-07	-
Collapsibility potential	$\varepsilon_{v,col}$	%	2 (loose) – 8 (very loose)	-	-	-	-	-
Saturation collapse start	S_{start}	%	30	-	-	-	-	-
Saturation collapse end	S_{end}	%	50	-	-	-	-	-

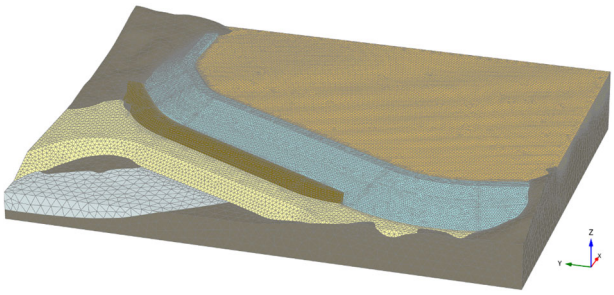

Figure 6. Model mesh at the final stage.

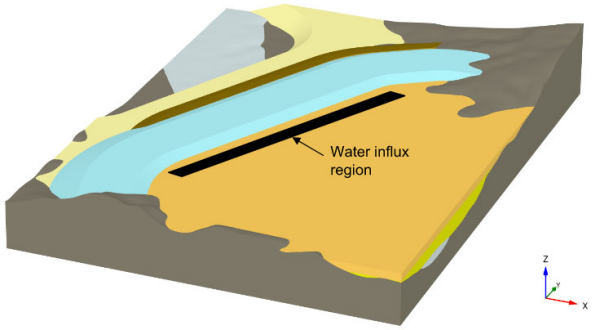

Figure 7. Water influx region as groundwater boundary condition.

5 RESULTS

Figure 8 shows settlements and plastic strains for the first raise embankment at tailings elevation at RL 572 m, after the hydro-mechanical deformation problem is solved. A diagonal concentration of plastic strains develops, likely indicating the onset of crack propagation, due to the heterogeneity of the embankment foundation. This contrast arises from the presence of a stiffer zone beneath the crest of the starter embankment and a softer zone associated with the underlying dumped waste fill. Notably, the same strain localization is observed even under completely dry conditions, suggesting that it would propagate regardless the hydraulic conditions, and driven not because of the water table and waste fill collapse, but due to the dam's geometric design.

The vertical displacements shown in the model crest for that tailings' elevation goes from 2 cm towards the north of the TSF and settlements around 1 cm in the southern region.

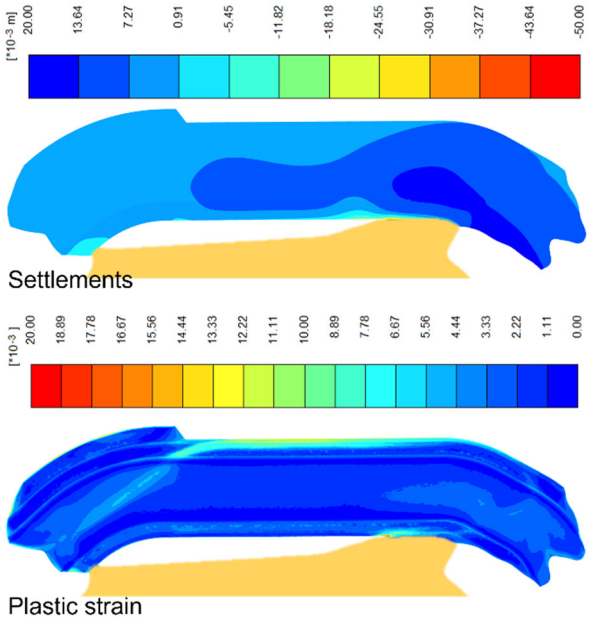

Figure 8. First raise embankment deformation and plastic strain at tailings elevation RL 572 m.

After the raise embankment is fully constructed and the tailings are raised to RL 577.5 m, they surpassed the loosely placed rockfill elevation, increasing their contact area. This phenomenon, combined with additional segregated slurry water, caused a rise in the water table, subjecting a larger portion of the rockfill to wetting-collapse strains. By RL 582 m, the fill in contact with the tailings had largely consolidated,

becoming less permeable and maintaining a nearly constant water table, with minimal additional collapse at the fill base. At subsequent elevations—RL 592 m and RL 602 m—the water table and wetting front at the base progressively drew down, as the tailings mass retained most of its interstitial water and gradually released it through the foundation. Nonetheless, the fill surface became partially saturated towards the upstream face, promoting additional deformations in that region.

Figure 9 show a plan view (top of model) of the loosely placed rockfill at tailings RL 582 m and Figure 10 the final stage of the tailings deposition at RL 602 m, displaying the saturation profile and volumetric strain produced by wetting collapse.

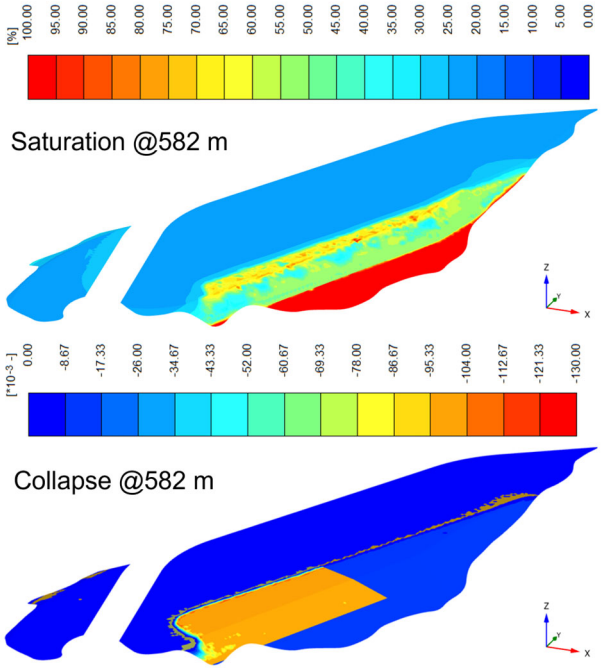

Figure 9. Rockfill collapse due to saturation at RL 582 m tailings deposition.

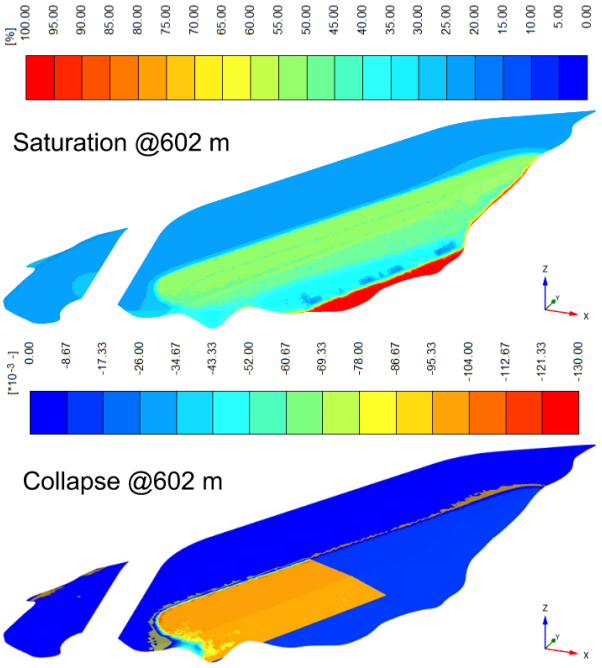

Figure 10. Rockfill collapse due to saturation at final tailings deposition.

Figure 11 shows the outcomes for settlements as well as strain concentration and plastic strain that may indicate preferential crack regions for the final tailings elevation at RL 602 m. By the end of the construction, the maximum vertical displacement towards the upstream abutment is 1.75 m, while the maximum crest settlement is about 1.2 m. These values suggest that ongoing maintenance may be required to preserve the crest level and maintain storage capacity. Propagation of transverse cracking is expected, extending its path along the downstream side parallel to the TSF crest. Other minor cracks on the upstream side are also anticipated, driven mainly by tailings deposition.

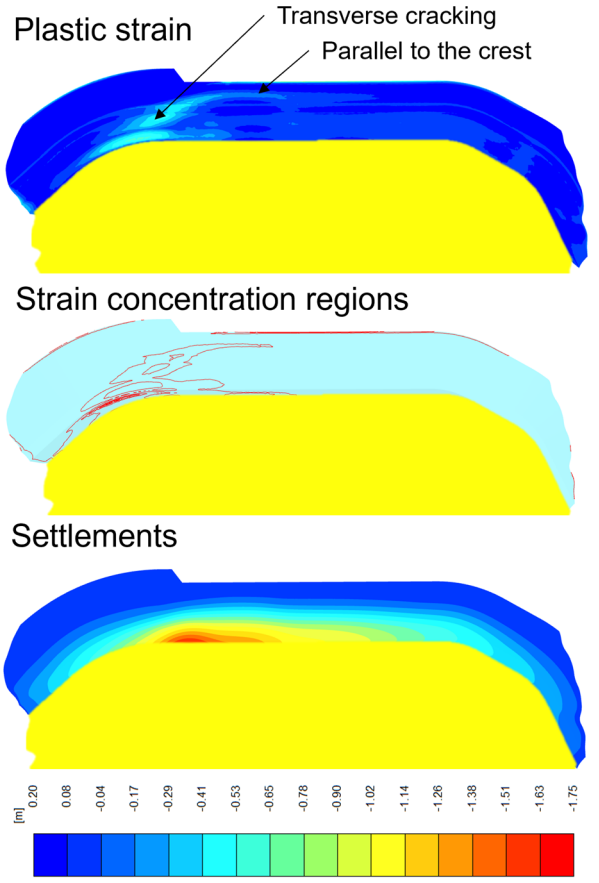

Figure 11. Strain concentration regions and settlements in the embankment at final tailings deposition.

The deformed configuration of the final-stage embankment is presented in Figure 12, with the tailings layer hidden to improve visualization. It is observed that the structure undergoes simultaneous torsion and vertical displacement due to loosely placed rockfill settling and self-weight consolidation of the tailings. These combined phenomena intensified the propagation of both transverse and longitudinal downstream cracks.

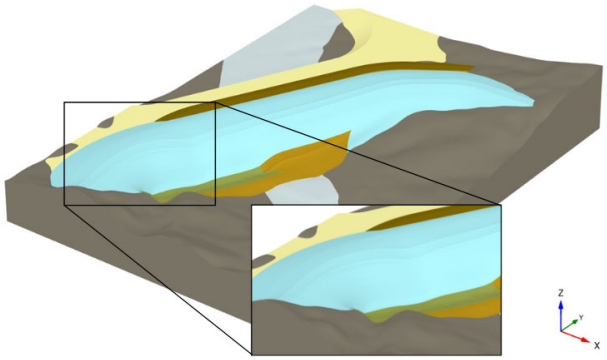

Figure 12. Deformed model (exaggerated 20 times) at final tailings deposition.

6 CONCLUSIONS

The paper presents a three-dimensional hydro-mechanical finite-element model of a downstream-raised tailings storage facility (TSF) built with dumped rockfill, implemented in PLAXIS 3D using a simple user-defined constitutive law that captures volumetric collapse upon increased saturation.

Laboratory calibration against large-strain triaxial and oedometer tests demonstrated that the model reliably reproduces stiffness, strength (peak friction angles of 37°–41°), and wetting-induced collapse magnitudes observed in controlled tests.

Application of the calibrated model to the staged construction sequence revealed significant deformation trends: a maximum upstream abutment displacement of 1.75 m and crest settlement of 1.2 m at final raise (RL 602 m), with collapse-driven strain concentrating along the downstream abutment—indicating likely crack initiation zones—and additional minor cracking on the upstream face due to tailings deposition and water table fluctuations. These findings underscore the value of integrating advanced numerical simulations into TSF design and monitoring. Predictive insight into deformation and crack propagation enables targeted maintenance—such as optimized compaction, drainage control, and crack remediation—to safeguard structural integrity and storage capacity. Future work should explore parametric sensitivities (e.g., PSD variations, raise rates, rainfall loading) and leverage real-time monitoring data to continuously refine the model's forecasting accuracy and support risk-informed tailings management.

7 REFERENCES

de Souza Neto, E. A., D. Peric, & D. R. J. Owen (2008). *The mathematical Theory of Plasticity*. John Wiley and Sons, Ltd.

Marsal, R. (1973). Mechanical properties of rockfill. *Embankment dam engineering, Casagrande volume (eds R.C. Hirschfeld and S.J. Poulos), John Wiley and Sons, New York*, 109–200.

Oldecop, L. & E. Alonso (2004). Testing rockfill under relative humidity control. *Geotechnical Testing Journal 27*(3), 269–278.

Oldecop, L. A. & E. E. Alonso (2001). A model for rockfill compressibility. *Géotechnique 51*(2), 127–139.

Sottile, M., N. Labanda, I. G. Mendive, O. Ledesma, &A. O. Sfriso (2019). A family of constitutive models implemented in Plaxis to simulate cemented mine backfill. *XVI Pan-American Conference on Soil Mechanics and Geotechnical Engineering (XVI PCSMGE)*, 576–584.

Sowers, G. F., R. C. Williams, & T. S. Wallace (1965). Compressibility of broken rock and the settlement of rockfills. *6th International Conference on Soil Mechanics and Foundation Engineering (Montreal)*, 561–565.